JACS
JOURNAL OF THE AMERICAN CHEMICAL SOCIETY
Article
pubs.acs.org/JACS

Dissociative Carbon Dioxide Adsorption and Morphological Changes on Cu(100) and Cu(111) at Ambient Pressures

Baran Eren,[†] Robert S. Weatherup,[†] Nikos Liakakos,[‡] Gabor A. Somorjai,[†,§] and Miquel Salmeron*[,†,∥]

[†]Materials Sciences Division and [‡]Chemical Sciences Division, Lawrence Berkeley National Laboratory, 1 Cyclotron Road, Berkeley, California 94720, United States

[§]Department of Chemistry, University of California, Berkeley, California 94720, United States

[∥]Department of Materials Science and Engineering, University of California, Berkeley, California 94720, United States

Supporting Information

ABSTRACT: Ambient-pressure X-ray photoelectron spectroscopy (APXPS) and high-pressure scanning tunneling microscopy (HPSTM) were used to study the structure and chemistry of model Cu(100) and Cu(111) catalyst surfaces in the adsorption and dissociation of CO_2. It was found that the (100) face is more active in dissociating CO_2 than the (111) face. Atomic oxygen formed after the dissociation of CO_2 poisons the surface by blocking further adsorption of CO_2. This "self-poisoning" mechanism explains the need to mix CO into the industrial feed for methanol production from CO_2, as it scavenges the chemisorbed O. The HPSTM images show that the (100) surface breaks up into nanoclusters in the presence of CO_2 at 20 Torr and above, producing active kink and step sites. If the surface is precovered with atomic oxygen, no such nanoclustering occurs.

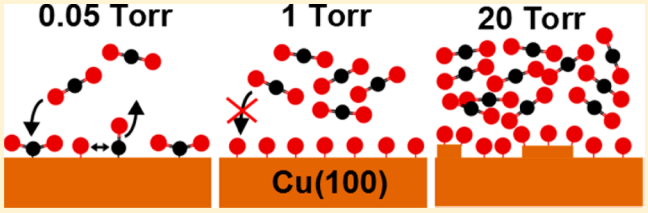

1. INTRODUCTION

Dissociative CO_2 adsorption on Cu surfaces is a key reaction step in heterogeneous catalysis of the reverse water gas shift (RWGS), i.e., $CO_2 + H_2 \rightleftarrows CO + H_2O$, and in methanol synthesis.[1,2] Recycling of CO_2 into methanol and other fuels is a possible way to address the persisting problem of increasing CO_2 emission that contributes to climate change.[3] When combined with other renewable sources (solar, wind, tidal, etc.) that can provide input energy, this reaction offers an attractive route for achieving independence from fossil fuels.[3] Although methanol synthesis involves mixtures of CO, H_2, and CO_2, carbon-labeling experiments have shown that CO_2 is the source of the carbon incorporated into methanol.[4,5] For all of these reasons, CO_2 adsorption on Cu surfaces has been the subject of many surface science studies. At low pressures, with gas exposures of a few langmuir (1 langmuir = 10^{-6} Torr·s), the most stable surface of Cu, with (111) orientation, was found to have no interaction with CO_2.[6] More active stepped and kinked surfaces, however, were found to dissociate CO_2 even at cryogenic temperatures.[7,8] The results in the literature are less clear regarding the Cu(110) surface, which appears to be less active than the stepped surfaces but more active than the (111) surface. For example, refs 8−11 report that no reaction occurs, whereas refs 12 and 13 claim that CO_2 dissociates into CO and O on the Cu(110) surface. At higher pressures and/or temperatures, CO_2 was found to dissociate slowly on Cu(111) but readily on Cu(100) and Cu(110).[14−16]

As suggested by Irvin Langmuir, the general approach in heterogeneous catalysis of studying "checkerboard surfaces" (single crystals) as model systems for more complex "porous bodies" has provided the core of our current understanding of surfaces and surface reactions in the second half of the 20th century.[17−19] Many techniques based on electron and ion probes have been developed because of their high surface sensitivity. The main limitation of these techniques is that they require very low pressures and often cryogenic temperatures. Under these conditions, however, the surfaces of the materials may differ substantially from those at ambient pressures and temperatures because a high gas pressure can overcome the problem of low binding energies of many reactants and remove the limitation of slow kinetics imposed by low-temperature operation. Over the last decades, along with other groups, we have developed high-pressure scanning tunneling microscopy (HPSTM)[20−23] and ambient-pressure X-ray photoelectron spectroscopy (APXPS)[24−26] to access structural and chemical information on surfaces up to atmospheric and Torr pressure ranges, respectively. With these techniques we have shown that under ambient conditions many surfaces undergo large restructuring upon reactant adsorption,[27−29] with Cu being an especially important example because its low cohesive energy facilitates restructuring.[29]

In this study, we show that the dissociative adsorption of CO_2 on Cu(100) results in the formation of Cu clusters stabilized by the species formed upon exposure to pressures of 20 Torr and above at room temperature (RT). This indicates that the energy gained upon the dissociative adsorption of CO_2 is higher than the formation energy of the clusters, which

Received: April 20, 2016
Published: June 9, 2016

DOI: 10.1021/jacs.6b04039
J. Am. Chem. Soc. 2016, 138, 8207−8211

requires the breaking of Cu−Cu bonds. This finding is of fundamental importance for understanding the role of the catalyst surface under realistic conditions because, as we show here, even the initially flat surface, where the terrace atoms are highly coordinated, restructures at ambient pressures by forming numerous steps, kinks, and clusters, which are active sites for catalytic reactions. Moreover, the atomic oxygen produced by CO_2 dissociation poisons the surface and inhibits further CO_2 adsorption. This is underestimated in the literature, especially in microkinetics calculations, which assume an oxygen-free metallic surface throughout the reaction.[30−32] An exception is a recent study with APXPS, which also underlines the necessity of CO to remove atomic oxygen on nickel.[33] We also show that a surface reconstructed with oxygen does not break up into clusters because of its already low surface energy. This finding highlights the importance of CO in the industrial gas mixture for methanol synthesis because it reacts away the chemisorbed O responsible for deactivating the catalyst.

2. METHODS

2.1. Preparation. Clean Cu surfaces were prepared by several cycles of Ar sputtering (1 keV, 15 min) and annealing (793−823 K, 10 min). The clean Cu(100) surface was exposed to 1000 langmuir of O_2 at 520 K to obtain a Cu(100)-($\sqrt{2} \times 2\sqrt{2}$)R45°-O surface reconstruction.[34,35] The large exposure likely results in some amount of oxygen being dissolved in the near-surface region of the crystal.[35] Research-grade (99.998% purity) CO_2 gas was leaked into the measurement chambers, while the pressure was measured with an MKS 722A Baratron capacitance pressure gauge.

2.2. HPSTM. HPSTM measurements were performed at RT with a home-built scanning tunneling microscope[22] using Pt/Ir tips. The microscope was operated in constant-current mode with the bias voltage applied to the sample. The imaging parameters are indicated in the figure captions. Images were taken at ultrahigh vacuum (UHV) (1×10^{-10} Torr) or 1 or 20 Torr CO_2 approximately 15 min after gas dosing.

2.3. APXPS. APXPS experiments were performed at beamline (BL) 11.0.2 of the Advanced Light Source (ALS), the Berkeley Lab Synchrotron Facility, at a base pressure of 4×10^{-10} Torr. Photon energies were adjusted to yield photoelectrons with kinetic energies of around 200 eV in the O 1s, C 1s, and Cu 2p regions. O 1s and C 1s spectra were acquired ∼3 and ∼4 min after CO_2 dosing, respectively. The peak positions were referenced to the Fermi level, measured in the same spectrum. Peak areas and widths were measured from Doniach−Šunjić fits to the spectra. Spectra were collected at RT at 0.05, 0.3, and 1 Torr CO_2 and at 0.3 Torr CO_2 after the sample was kept at 10 Torr for 5 min. To minimize the effects of beam-induced CO_2 dissociation, we defocused the X-ray beam. After acquisition of each spectrum (in less than half a minute), the position of the beam spot on the sample was changed to minimize beam effects. Further measurements performed at BL 9.3.2 of the ALS (at a base pressure of 1×10^{-9} Torr) are shown in the Supporting Information.

3. RESULTS AND DISCUSSION

3.1. Adsorbed Species and Coverage on Different Cu Faces. Bond breaking upon chemisorption is probably one of the most important roles of a catalyst surface.[19] In order to investigate the role of surface structure, we conducted experiments on the two lowest-index Cu surfaces. On the (111) surface, CO_2 adsorbs as $CO_2^{\delta-}$, which produces XPS peaks at 531.4 and 288.4 eV.[36−39] The two lower panels of Figure 1 show the O 1s and C 1s regions of XPS spectra acquired in the presence of 0.05 and 0.3 Torr CO_2 at RT. The peak around 529.7−529.8 eV is due to atomic oxygen,[35] which can have two origins: CO_2 dissociation and residual O_2 gas in

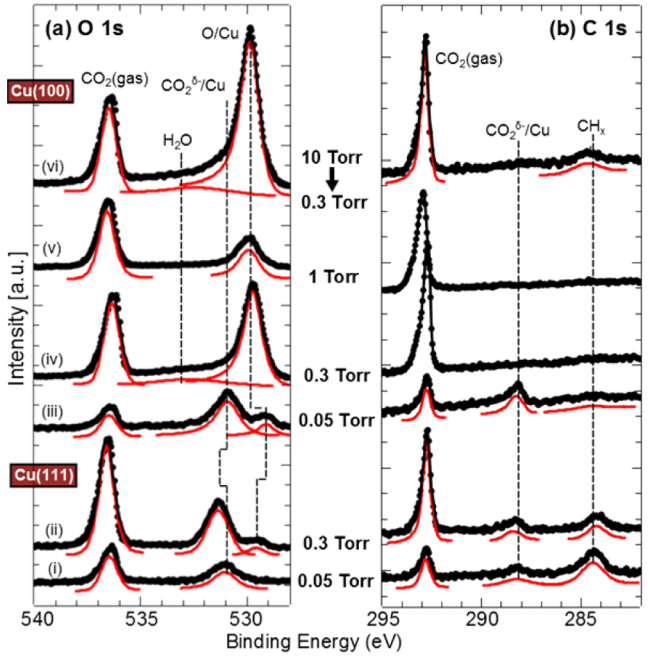

Figure 1. (a) O 1s and (b) C 1s regions of the APXPS spectra in the presence of CO_2 at RT on the Cu(111) surface (lower two panels) and on the Cu(100) surface (upper four panels): (i, iii) 0.05 Torr CO_2; (ii, iv) 0.3 Torr CO_2; (v) 1 Torr CO_2; (vi) 0.3 Torr CO_2 after the sample was kept for 5 min in 10 Torr CO_2. The peaks above 536 and 292 eV (different in each spectrum due to the different work functions) are from gas-phase CO_2. CO_2 adsorbs as $CO_2^{\delta-}$ and produces the peaks at 531.4 and 288.4 eV. The atomic oxygen peak appears at ∼529.8 eV. However, at low coverage (e.g., in the presence of 0.05 Torr CO_2) we observe both the $CO_2^{\delta-}$ and atomic oxygen peaks at around 0.4 eV lower binding energies in the O 1s region, which we attribute to stronger interactions with the metal surface. CH_x and water contamination produce the peaks at 284.2−284.7 and 532.5−533.0 eV, respectively. The former typically appears in the absence of atomic oxygen, and the latter typically appears in the presence of atomic oxygen on the surface. The background-corrected (Shirley for adsorbed species, linear for gas-phase species) and fitted Doniach−Šunjić curves (red) are displaced vertically downward for clarity. The black lines through the experimental data (dots) are the sums of the fitting curves.

the background. Even though the amount of O_2 is of the order of parts per million in CO_2, its high reactivity compared with that of CO_2 may be enough to produce a small coverage on the surface.[34,35] At low coverage (e.g., 0.05 Torr), both the $CO_2^{\delta-}$ and atomic oxygen peaks shift 0.4 eV toward lower binding energy, which we attribute to stronger interactions with the underlying metal. Besides the peaks due to $CO_2^{\delta-}$ and atomic oxygen, small contamination peaks at around 532.5−533 and 284.2−284.7 eV from water and hydrocarbons, respectively, were also sometimes observed as a result of residual gases in the chamber and gas cylinder.[40]

The O 1s and C 1s regions of the XPS spectra obtained on Cu(100) in the presence of CO_2 at RT are shown in the upper four panels in Figure 1. While $CO_2^{\delta-}$ was observed at 0.05 Torr, indicating molecular adsorption, remarkably no $CO_2^{\delta-}$ was detected on the Cu(100) surface at 0.3 Torr and above, while the atomic oxygen coverage increased with CO_2 pressure. Table 1 summarizes the $CO_2^{\delta-}$ and atomic oxygen coverages reached 3 min after dosing of gas at different pressures. Literature values of the activation energy for CO_2 dissociation are 1.33−1.36 eV on Cu(111),[41,42] 0.96 eV on Cu(100),[43] and

DOI: 10.1021/jacs.6b04039
J. Am. Chem. Soc. 2016, 138, 8207−8211

Table 1. Coverages of $CO_2^{\delta-}$ and Atomic Oxygen on the Cu(111) and Cu(100) Surfaces at RT as Functions of the CO_2 Pressure Obtained ~3 min after Gas Dosing[a]

	P (Torr)	θ_{CO_2} (ML)	θ_O (ML)
Cu(111)	0.05	0.03	0
	0.3	0.085	0.04
Cu(100)	0.05	0.085	0.08
	0.3	0	0.34
	1	0	0.42
	10[b]	0	0.61

[a]The results do not represent steady-state coverage, but changes (increases in O_{ads} intensity) occur very gradually because of the slow kinetics at RT. Coverage estimation was done using the O 1s to Cu 2p XPS intensity ratio and the known 0.5 ML coverage of the Cu(100)-($\sqrt{2} \times 2\sqrt{2}$)R45°-O structure as a reference after removal of the subsurface component in the O 1s spectra (Figure S3). [b]Measurement at 0.3 Torr after the Cu(100) surface was kept for 5 min at 10 Torr with the X-ray beam blanked and then the pressure was decreased to 0.3 Torr. This was due to limitations of the APXPS setup used that make acquisition of XPS spectra above 1 Torr challenging.

0.67 eV on Cu(110).[16] At stepped and kinked surfaces, CO_2 dissociation occurs even at cryogenic temperatures.[8,7] Our results in Figure 1 (and in Figure S1 for Cu(110)) confirm the strong dependence of the dissociative activation energy on the coordination number of the Cu atoms. The results also show that no CO_2 can adsorb on a Cu surface after it is covered with atomic oxygen through CO_2 dissociation. This "self-poisoning" explains the need for CO in the industrial feed for methanol synthesis, because it removes oxygen from the surface. Another interesting observation is that the atomic oxygen coverage can exceed 0.5 monolayer (ML) (Table 1), which we associate with the breakup of the surface into nanoclusters, as shown by STM (see the next section).

Since Cu(100) is more active than Cu(111) for CO_2 dissociation, we selected this surface for further APXPS and HPSTM studies. The amount of chemisorbed O is determined by the $CO_2(g) \rightleftarrows O_{ads} + CO(g)$ equilibrium reaction. Using the O 1s to Cu 2p XPS intensity ratio in the well-established Cu(100)-($\sqrt{2} \times 2\sqrt{2}$)R45°-O surface reconstruction as a reference, we calculated the atomic oxygen coverage at 1 Torr CO_2 to be 0.42 ML (coverages at other pressures are summarized in Table 1). Since the base pressure in the APXPS chamber was 4 times higher than that in the HPSTM chamber and there was always some X-ray-beam-induced dissociation, the coverage of 0.42 ML at 1 Torr is expected to be a slight overestimation. We note that if present, both carbonate formation (peaks at 531.9 and 289.3 eV)[38] and CO_{ads} as a reaction intermediate remained below the XPS detection limit.

3.2. Structural Changes on the Cu(100) Surface. Figure 2 shows STM images of the Cu(100) surface in the presence of 1 Torr CO_2. In the low-magnification image (a), the surface consists of flat terraces separated by steps, as in UHV. At higher magnification (b, c), we observe the surface covered with a fraction of a monolayer of atomic oxygen, which appears as dark spots (depressions in STM contrast). This type of "disordered" atomic oxygen does not induce reconstruction of the Cu surface, and it is easy to remove with CO,[44] which is desirable for methanol synthesis as it allows the metallic catalyst surface to be easily regenerated.

When the CO_2 pressure is increased by a factor of 20, the surface is significantly altered (Figure 3). The initially large and

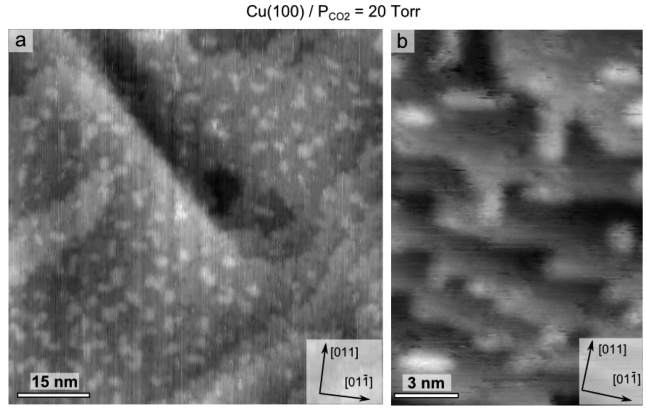

Figure 3. HPSTM images of the Cu(100) surface in the presence of 20 Torr CO_2 at RT. The surface breaks up into clusters, roughly half of them with edges oriented along ⟨011⟩ directions. Imaging conditions: (a) I_t = 1 nA, V_b = 0.15 V; (b) I_t = 0.5 nA, V_b = 0.4 V.

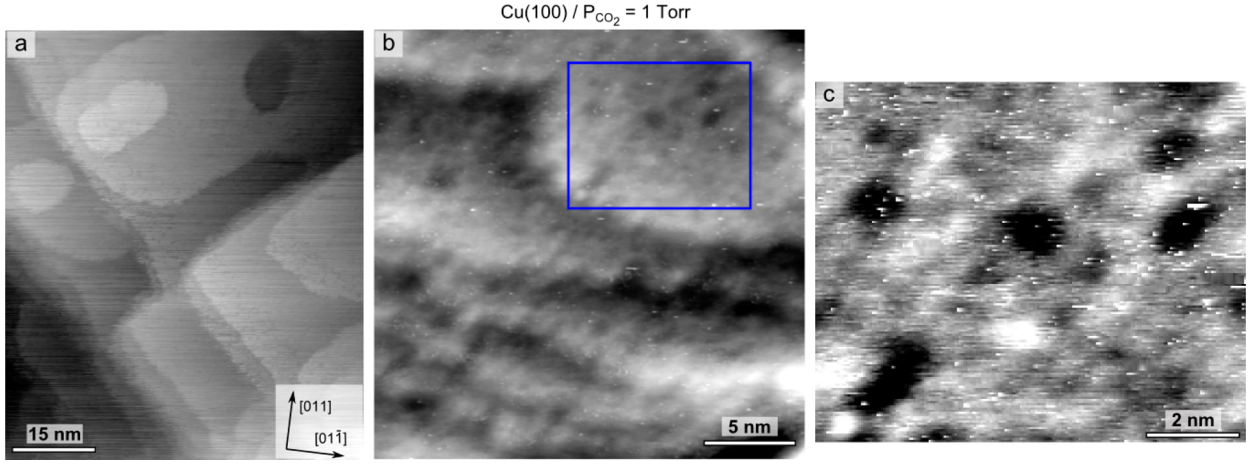

Figure 2. HPSTM images of the Cu(100) surface in the presence of 1 Torr CO_2 at RT. (a) Large-scale image showing the surface consisting of flat terraces separated by steps, as found in UHV (I_t = 1 nA, V_b = 0.15 V). Unlike in UHV however, the surface is covered with dark spots due to O atoms (depressions in tunneling contrast). (b) Higher-magnification image showing more clearly the dark spots due to O atoms (I_t = 1 nA, V_b = −0.25 V). (c) Further magnification of the framed area in (b).

DOI: 10.1021/jacs.6b04039
J. Am. Chem. Soc. 2016, 138, 8207−8211

flat terraces are now covered with one-atom-high clusters. Roughly half of the cluster edges are oriented along ⟨011⟩ directions (i.e., equivalent [011] and [01$\bar{1}$] directions) while the other half show no preferential orientation. The clusters are formed by Cu atoms detached from the steps. In recent studies we showed that the Cu(100) surface breaks up in the presence of pure CO gas as a result of the lowering of Cu−Cu cohesion caused by adsorbed CO and the energy gain of CO adsorption on low-coordination sites.[45] However, in the case of pure CO, all of the cluster and step edges align along ⟨001⟩ directions (i.e., equivalent [001] and [010] directions).[45] The formation of nanoclusters in the present study can be explained as a result of the energy gain from binding of the oxygen atoms from dissociated CO_2, which offsets the energy to detach Cu atoms from the step edges. However, CO is not bound to the clusters at RT because of its low adsorption energy, so only atomic oxygen remains on the surface. Because of the increased surface area, the nominal coverage of oxygen can exceed 0.5 ML. We also note that an ordered surface structure such as the Cu(100)-($\sqrt{2} \times 2\sqrt{2}$)R45° structure is not observed here. We attribute this to kinetic limitations at RT (i.e., RT is probably insufficient to displace one of every four Cu atoms to form the aforementioned reconstruction) as well as some parts of the surface (most likely the cluster edges) being oxidized to Cu_2O (Figure S4).

3.3. Interaction of CO_2 with the Cu(100)-($\sqrt{2} \times 2\sqrt{2}$)R45°-O Surface. We used the oxygen-covered Cu(100)-($\sqrt{2} \times 2\sqrt{2}$)R45° surface as our second model system. Figure 4a,b shows large-scale and atomically resolved

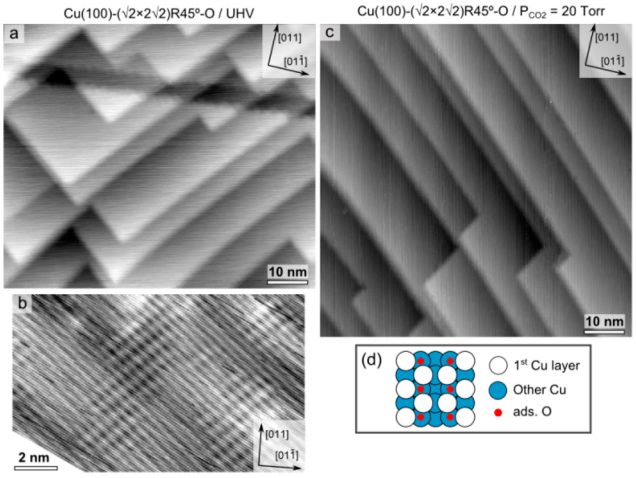

Figure 4. (a, b) HPSTM images of the Cu(100)-($\sqrt{2} \times 2\sqrt{2}$)R45°-O surface in UHV. In (a), all the step edges are oriented along the ⟨001⟩ directions. (b) Expanded image showing the atomically resolved structure.[34,47] (c) Image of the same surface in the presence of 20 Torr CO_2, showing that no changes occur under this CO_2 pressure. (d) Ball model of the Cu(100)-($\sqrt{2} \times 2\sqrt{2}$)R45°-O structure. The imaging parameters are I_t = 0.5 nA and V_b = 0.5 V for all of the images.

images of the surface in UHV, and a ball model of the periodic surface structure is shown in Figure 4d. All of the steps appear to be oriented along the ⟨001⟩ directions. A few steps appear to be oriented along ⟨011⟩ directions at low resolution (dark band near the top of Figure 4a) but actually consist of a sawtooth structure with ⟨001⟩-oriented edges (Figure S5). Since the surface is already saturated with atomic oxygen there can be no further gain in energy through adsorption of atomic oxygen from CO_2 dissociation.[46]

In the presence of 0.3 Torr CO_2, no $CO_2^{\delta-}$ was detectable with APXPS as in the case of the initially bare sample (Figure S2). Figure 4c shows the same surface under 20 Torr CO_2. As can be seen, the orientation of the steps remains unchanged and no clusters appear on the surface, from which we conclude that the oxygen-induced reconstruction remains intact and completely passivates the surface at least up to 20 Torr CO_2.

4. CONCLUSIONS

We have shown that the adsorption of CO_2 on Cu(100) at RT is molecular at 0.05 Torr but dissociative at 0.3 Torr and above, likely as a result of slow kinetics. On the less active Cu(111) surface, the CO_2 adsorption is still molecular at 0.3 Torr. Atomic oxygen produced by CO_2 dissociation poisons the surface when it reaches a coverage of $>^1/_3$ ML. This "self-poisoning" mechanism explains the need for CO in the industrial feed used for the synthesis of methanol from CO_2 as a means of removing atomic oxygen. At 1 Torr CO_2, atomic oxygen from dissociative adsorption produces dark spots (depressions in tunneling contrast) in HPSTM images. In the presence of 20 Torr CO_2, the Cu(100) surface breaks up into clusters, whereas on an oxygen-saturated surface no such nano clustering occurs because of the aforementioned poisoning and the resulting lack of CO_2 adsorption. These observations provide new insights at the molecular level into the "self-poisoning" and the abundance and role of step and kink sites in RWGS and methanol synthesis reactions catalyzed by Cu-based materials.

■ ASSOCIATED CONTENT

Supporting Information

The Supporting Information is available free of charge on the ACS Publications website at DOI: 10.1021/jacs.6b04039.

Additional APXPS spectra, STM image of the sawtooth step edge, and Cu L_3 edge of the NEXAFS spectra (PDF)

■ AUTHOR INFORMATION

Corresponding Author

*mbsalmeron@lbl.gov

Notes

The authors declare no competing financial interest.

■ ACKNOWLEDGMENTS

This work was supported by the Office of Basic Energy Sciences (BES), Division of Materials Sciences and Engineering, U.S. Department of Energy (DOE), under Contract DE-AC02-05CH11231 through the Chemical and Mechanical Properties of Surfaces, Interfaces and Nanostructures Program (FWP: KC3101). It used resources of the Advance Light Source, which is supported by the DOE Office of Science. R.S.W. acknowledges a Research Fellowship from St. John's College, Cambridge, and a Marie Skłodowska-Curie Individual Fellowship (Global) under Grant ARTIST (656870) from the European Union's Horizon 2020 Research and Innovation Programme. We thank Dr. Hendrik Bluhm and Dr. Ethan Crumlin for assistance with the experiments at the Advanced Light Source.

DOI: 10.1021/jacs.6b04039
J. Am. Chem. Soc. 2016, 138, 8207−8211

REFERENCES

(1) Rasmussen, P. B.; Holmblad, P. M.; Askgaard, T.; Ovesen, C. V.; Stoltze, P.; Nørskov, J. K.; Chorkendorff, I. *Catal. Lett.* **1994**, *26*, 373.
(2) Schumacher, N.; Andersson, K.; Grabow, L. C.; Mavrikakis, M.; Nerlov, J.; Chorkendorff, I. *Surf. Sci.* **2008**, *602*, 702−711.
(3) Olah, G. A. *Angew. Chem., Int. Ed.* **2013**, *52*, 104−107.
(4) Chinchen, G. C.; Denny, P. J.; Parker, D. G.; Spencer, M. S.; Whan, D. A. *Appl. Catal.* **1987**, *30*, 333−338.
(5) Chinchen, G. C.; Denny, P. J.; Jennings, J. R.; Spencer, M. S.; Waugh, K. C. *Appl. Catal.* **1988**, *36*, 1−65.
(6) Habraken, F. H. P. M.; Kieffer, E. Ph.; Bootsma, G. A. *Surf. Sci.* **1979**, *83*, 45−59.
(7) Bönicke, I. A.; Kirstein, W.; Thieme, F. *Surf. Sci.* **1994**, *307*−*309*, 177−181.
(8) Fu, S. S.; Somorjai, G. A. *Surf. Sci.* **1992**, *262*, 68−76.
(9) Krause, J.; Borgmann, D.; Wedler, G. *Surf. Sci.* **1996**, *347*, 1−10.
(10) Ernst, K.-H.; Schlatterbeck, D.; Christmann, K. *Phys. Chem. Chem. Phys.* **1999**, *1*, 4105−4112.
(11) Funk, S.; Hokkanen, B.; Wang, J.; Burghaus, U.; Bozzolo, G.; Garcés, J. E. *Surf. Sci.* **2006**, *600*, 583−590.
(12) Wachs, I. E.; Madix, R. J. *J. Catal.* **1978**, *53*, 208−227.
(13) Schneider, T.; Hirschwald, W. *Catal. Lett.* **1992**, *14*, 197−205.
(14) Campbell, C. T.; Daube, K. A.; White, J. M. *Surf. Sci.* **1987**, *182*, 458−476.
(15) Rasmussen, P. B.; Taylor, P. A.; Chorkendorff, I. *Surf. Sci.* **1992**, *269*−*270*, 352−359.
(16) Nakamura, J.; Rodriguez, J. A.; Campbell, C. T. *J. Phys.: Condens. Matter* **1989**, *1*, SB149.
(17) Langmuir, I. *Trans. Faraday Soc.* **1922**, *17*, 607−620.
(18) Somorjai, G. A. *Introduction to Surface Chemistry and Catalysis*; Wiley-VCH: New York, 1999.
(19) Ertl, G. *Angew. Chem., Int. Ed.* **2008**, *47*, 3524−3535.
(20) McIntyre, B. J.; Salmeron, M.; Somorjai, G. A. *Rev. Sci. Instrum.* **1993**, *64*, 687−691.
(21) Laegsgaard, E.; Osterlund, L.; Thostrup, P.; Rasmussen, P. B.; Stensgaard, I.; Besenbacher, F. *Rev. Sci. Instrum.* **2001**, *72*, 3537−3542.
(22) Tao, F.; Tang, D.; Salmeron, M.; Somorjai, G. A. *Rev. Sci. Instrum.* **2008**, *79*, 084101.
(23) Besenbacher, F.; Thostrup, P.; Salmeron, M. *MRS Bull.* **2012**, *37*, 677−681.
(24) Salmeron, M.; Schlögl, R. *Surf. Sci. Rep.* **2008**, *63*, 169−199.
(25) Salmeron, M. *MRS Bull.* **2013**, *38*, 650−667.
(26) Tao, F.; Salmeron, M. *Science* **2011**, *331*, 171−174.
(27) Tao, F.; Dag, S.; Wang, L.-W.; Liu, Z.; Butcher, D. R.; Salmeron, M.; Somorjai, G. A. *Nano Lett.* **2009**, *9*, 2167−2171.
(28) Tao, F.; Dag, S.; Wang, L.-W.; Liu, Z.; Butcher, D. R.; Bluhm, H.; Salmeron, M.; Somorjai, G. A. *Science* **2010**, *327*, 850−853.
(29) Eren, B.; Zherebetskyy, D.; Patera, L. L.; Wu, C. H.; Bluhm, H.; Africh, C.; Wang, L.-W.; Somorjai, G. A.; Salmeron, M. *Science* **2016**, *351*, 475−478.
(30) Behrens, M.; Studt, F.; Kasatkin, I.; Kühl, S.; Hävecker, M.; Abild-Pedersen, F.; Zander, S.; Girgsdies, F.; Kurr, P.; Kniep, B. L.; Tovar, M.; Fischer, R. W.; Nørskov, J. K.; Schlögl, R. *Science* **2012**, *336*, 893−897.
(31) Grabow, L. C.; Mavrikakis, M. *ACS Catal.* **2011**, *1*, 365−384.
(32) Studt, F.; Behrens, M.; Kunkes, E. L.; Thomas, N.; Zander, S.; Tarasov, A.; Schumann, J.; Frei, E.; Varley, J. B.; Abild-Pedersen, F.; Nørskov, J. K.; Schlögl, R. *ChemCatChem* **2015**, *7*, 1105−1111.
(33) Monachino, E.; Greiner, M.; Knop-Gericke, A.; Schlögl, R.; Dri, C.; Vesselli, E.; Comelli, G. *J. Phys. Chem. Lett.* **2014**, *5*, 1929−1934.
(34) Leibsle, F. M. *Surf. Sci.* **1995**, *337*, 51−66.
(35) Eren, B.; Lichtenstein, L.; Wu, C. H.; Bluhm, H.; Somorjai, G. A.; Salmeron, M. *J. Phys. Chem. C* **2015**, *119*, 14669−14674.
(36) Copperthwaite, R. G.; Davies, P. R.; Morris, M. A.; Roberts, M. W.; Ryder, R. A. *Catal. Lett.* **1988**, *1*, 11−20.
(37) Freund, H.-J.; Roberts, M. W. *Surf. Sci. Rep.* **1996**, *25*, 225−273.
(38) Deng, X.; Verdaguer, A.; Herranz, T.; Weis, C.; Bluhm, H.; Salmeron, M. *Langmuir* **2008**, *24*, 9474−9478.
(39) Eren, B.; Heine, Ch.; Bluhm, H.; Somorjai, G. A.; Salmeron, M. *J. Am. Chem. Soc.* **2015**, *137*, 11186−11190.
(40) Residual gases in the research-grade CO_2 cylinder: O_2, <2 ppm; H_2O, <3 ppm; N_2, <10 ppm; THC, <4 ppm; CO, <0.5 ppm. See: www.praxair.com.
(41) Gokhale, A. A.; Dumesic, J. A.; Mavrikakis, M. *J. Am. Chem. Soc.* **2008**, *130*, 1402−1414.
(42) Muttaqien, F.; Hamamoto, Y.; Inagaki, K.; Morikawa, Y. *J. Chem. Phys.* **2014**, *141*, 034702.
(43) Taylor, P. A.; Rasmussen, P. B.; Chorkendorff, I. *J. Vac. Sci. Technol., A* **1992**, *10*, 2570−2575.
(44) Xu, F.; Mudiyanselage, K.; Baber, A. E.; Soldemo, M.; Weissenrieder, J.; White, M. G.; Stacchiola, D. J. *J. Phys. Chem. C* **2014**, *118*, 15902−15909.
(45) Eren, B.; Zherebetskyy, D.; Hao, Y.; Patera, L. L.; Wang, L.-W.; Somorjai, G. A.; Salmeron, M. *Surf. Sci.* **2016**, *651*, 210−214.
(46) Soon, A.; Todorova, M.; Delley, B.; Stampfl, C. *Phys. Rev. B: Condens. Matter Mater. Phys.* **2006**, *73*, 165424.
(47) Baykara, M. Z.; Todorović, M.; Mönig, H.; Schwendemann, T. C.; Ünverdi, Ö; Rodrigo, L.; Altman, E. I.; Pérez, R.; Schwarz, U. D. *Phys. Rev. B: Condens. Matter Mater. Phys.* **2013**, *87*, 155414.

DOI: 10.1021/jacs.6b04039
J. Am. Chem. Soc. 2016, 138, 8207−8211